Atmos. Chem. Phys., 12, 7351–7363, 2012
www.atmos-chem-phys.net/12/7351/2012/
doi:10.5194/acp-12-7351-2012

Atmospheric Chemistry and Physics

Mixing of dust and NH_3 observed globally over anthropogenic dust sources

P. Ginoux[1], L. Clarisse[2], C. Clerbaux[2,3], P.-F. Coheur[2], O. Dubovik[4], N. C. Hsu[5], and M. Van Damme[2]

[1]NOAA Geophysical Fluid Dynamics Laboratory, Princeton, New Jersey, USA
[2]Spectroscopie de l'Atmosphère, Service de Chimie Quantique et Photophysique, Université Libre de Bruxelles, Brussels, Belgium
[3]UPMC Université Paris 06; Université Versailles St.-Quentin; CNRS/INSU, LATMOS-IPSL, Paris, France
[4]Laboratoire d'Optique Atmosphérique, Université de Lille 1/CNRS, Villeneuve d'Ascq, France
[5]NASA Goddard Space Flight Center, Greenbelt, Maryland, USA

Correspondence to: P. Ginoux (paul.ginoux@noaa.gov)

Received: 20 April 2012 – Published in Atmos. Chem. Phys. Discuss.: 16 May 2012
Revised: 1 August 2012 – Accepted: 3 August 2012 – Published: 16 August 2012

Abstract. The global distribution of dust column burden derived from MODIS Deep Blue aerosol products is compared to NH_3 column burden retrieved from IASI infrared spectra. We found similarities in their spatial distributions, in particular their hot spots are often collocated over croplands and to a lesser extent pastures. Globally, we found 22 % of dust burden collocated with NH_3, with only 1 % difference between land-use databases. This confirms the importance of anthropogenic dust from agriculture. Regionally, the Indian subcontinent has the highest amount of dust mixed with NH_3 (26 %), mostly over cropland and during the pre-monsoon season. North Africa represents 50 % of total dust burden but accounts for only 4 % of mixed dust, which is found over croplands and pastures in Sahel and the coastal region of the Mediterranean. In order to evaluate the radiative effect of this mixing on dust optical properties, we derive the mass extinction efficiency for various mixtures of dust and NH_3, using AERONET sunphotometers data. We found that for dusty days the coarse mode mass extinction efficiency decreases from 0.62 to 0.48 $m^2\,g^{-1}$ as NH_3 burden increases from 0 to 40 $mg\,m^{-2}$. The fine mode extinction efficiency, ranging from 4 to 16 $m^2\,g^{-1}$, does not appear to depend on NH_3 concentration or relative humidity but rather on mineralogical composition and mixing with other aerosols. Our results imply that a significant amount of dust is already mixed with ammonium salt before its long range transport. This in turn will affect dust lifetime, and its interactions with radiation and cloud properties.

1 Introduction

Mineral dust affects climate by absorbing and scattering solar and terrestrial radiation, by modifying cloud properties, and by interacting with ozone chemistry and the biosphere (Forster et al., 2007). The amplitude of these effects depends on the size, optical and chemical properties of dust. These properties may be considerably modified when dust is mixed with other aerosol types. In the case of dust mixed with ammonium salts, (1) the amount of solar absorption will decrease (Bauer et al., 2007), (2) the activation of cloud condensation nuclei will increase (Levin et al., 1996), (3) the activation of ice nucleation sites will decrease (Sullivan et al., 2010), (4) the recycling of NO_x is suppressed reducing pollution influence on surface ozone (Fairlie et al., 2010), and (5) iron dissolution which enhances ocean fertilization will increase (Meskhidze et al., 2003). Therefore, it is crucial to determine the mixing state of dust in order to better understand its effects on climate.

In situ observations have shown that ammonium salts commonly accumulate on dust particles (Galy-Lacaux et al., 2001; Jordan et al., 2003; Sullivan et al., 2007; Shi et al., 2008). The coating of dust particles by sulfate occurred by in-cloud processes, by which reactions with sulfuric acid (H_2SO_4) initiate the deposition of sulfate on the surface of the particles (Levin et al., 1996). Other mixing processes include coagulation of sulfate particles or oxidation of sulfur dioxide (SO_2) to sulfate on the particle surface

in the presence of ammonia (NH_3). The latter process involves titration of NH_3 by H_2SO_4 to form ammonium sulfate $(NH_4)_2SO_4$, ammonium bisulfate $(NH_4)SO_4$, or triammonium hydrogen disulfate $(NH_4)_3H(SO_4)_2$. Similarly, in presence of nitric acid (HNO_3), NH_3 will produce ammonium nitrate (NH_3NO_3) (Usher et al., 2003). Sulfate coatings on dust undergo efflorescence (crystallization) at different relative humidities depending on the size and mineralogy of dust (Usher et al., 2003).

By analyzing Asian dust, Sullivan et al. (2007) showed that transport pathways of dust through source of pollutants is more important than reaction kinetics in determining which species accumulate on dust. The scarcity of in-situ observations makes it difficult to extrapolate the predominance of dust mixing with pollutants at global scale, such that the impact of such mixing on climate is evaluated using poorly constrained models (Lesins et al., 2002; Bauer et al., 2007).

Using the Moderate Resolution Imaging Spectroradiometer (MODIS) Deep Blue satellite products, Ginoux et al. (2010) have retrieved global dust sources at 0.1° resolution. By comparing their location with land-use fraction, Ginoux et al. (2012) have calculated that 25 % of dust is emitted from agriculture, and called such dust as *anthropogenic*. Meanwhile, Clarisse et al. (2009) have retrieved the global distribution of ammonia (NH_3) from the Infrared Atmospheric Sounding Interferometer (IASI) infrared spectra and have shown that hot spots are often associated with agriculture. There is a remarkable similarity in the observed distribution of these hot spots and anthropogenic dust sources, which may provide the first evidence of co-located pollutants and dust over their sources (see Sect. 3). This would first confirm the existence of anthropogenic dust (Sect. 4), once our results have been validated (Sect. 5), and second that anthropogenic dust has different chemical and optical properties (Sect. 6). The implications of these results on our understanding of the effects of dust on climate are discussed in Sect. 7.

2 Satellite data

2.1 Dust column burden

The MODIS instrument on the polar orbiting Aqua satellite measures daily backscattering radiances globally since 2002. The MODIS Deep Blue algorithm employs radiances from the blue channels of MODIS instruments. At these wavelengths the surface reflectance is very low so that the presence of aerosol is detected by an increase of total reflectance and enhanced spectral contrast (Hsu et al., 2004, 2006). The values of AOD and single scattering albedo (ω) at 412, 470, 550 and 670 nm, and the Angstrom exponent (α) between 412 and 470 nm are retrieved at the pixel level over bright surfaces (reflectance at 550 nm greater than 0.15), and then averaged on a 10 by 10 km grid. The data are aggregated into granules forming the Level 2 data. These data are interpolated by surface-weighted averaging on a 0.1° by 0.1° regular latitude/longitude grid. Ginoux et al. (2012) extracted Dust Optical Depth (DOD) from MODIS collection 5.1 Level 2 (M-DB2) aerosol products by requiring the values of the Angstrom exponent to be less than 0, and the single scattering albedo to increase with wavelength. By analyzing 7 yr of daily global DOD, Ginoux et al. (2012) also found that globally 24 % of dust is emitted from sources associated with land-use fraction greater than 30 %, which they defined as anthropogenic. They also found very large variations between continents and seasons.

They validated M-DB2 DOD by comparing with AERONET data. They showed significant correlation between M-DB2 and AERONET data, with root mean square difference of 0.26 and mean absolute difference of 0.24. The largest biases were observed in California and Australia where M-DB2 largely overestimates DOD.

In the present study, we use daily global M-DB2 DOD from April 2009 to March 2010 and convert it into column burden. The conversion is performed following Ginoux et al. (2001) who expressed DOD (τ) and mass burden M by the following relation,

$$M = \frac{4}{3}\frac{\rho\, r_{\text{eff}}}{Q_{\text{ext}}}\tau = \frac{1}{\epsilon}\tau \quad (1)$$

where $r_{\text{eff}} = 1.2 \times 10^{-6}$ m is the effective radius, $\rho = 2600\,\text{kg m}^{-3}$ is the density of dust, $Q_{\text{ext}} = 2.5$ is the extinction efficiency at 550 nm and for a 1.2×10^{-6} particle radius, $\epsilon = 0.6\,\text{m}^2\,\text{g}^{-1}$ is the mass extinction efficiency, and τ is dust optical depth at 550 nm. The selection of r_{eff} is based on the effective radius of the total size distribution measured at Sal Island (Cape Verde) and Banizoumbou (Niger) by Tanré et al. (2001). As the aerosol optical depth increased, they observed that r_{eff} reaches 1.2×10^{-6} m at these two sites.

Such relation was also used by Kaufman et al. (2005) to convert DOD to M. Using $r_{\text{eff}} = 1.7 \times 10^{-6}$ m, $\rho = 2600\,\text{kg m}^{-3}$ and $Q_{\text{ext}} = 2.2$, they obtained $\epsilon = 0.37 \pm 0.05\,\text{m}^2\,\text{g}^{-1}$, which is 40 % lower than our value. On the other hand, our value is closer to the median value ($0.72\,\text{m}^2\,\text{g}^{-1}$) derived from global dust models (Huneeus et al., 2011). The range of values among these models is quite large, varying from 0.25 to $1.28\,\text{m}^2\,\text{g}^{-1}$. Similar range has been obtained from theoretical calculations (Hansell et al., 2011), with higher values associated with non-spherical particles. Also, values derived from field campaigns vary from 0.6 ± 0.1 at Barbados (Li et al., 1996) to 1.09 ± 0.4 at Cape Verde (Chen et al., 2011). There is clearly a need to better constrain ϵ, particularly over source areas where there are fewer data. This will be discussed in Sect. 5.

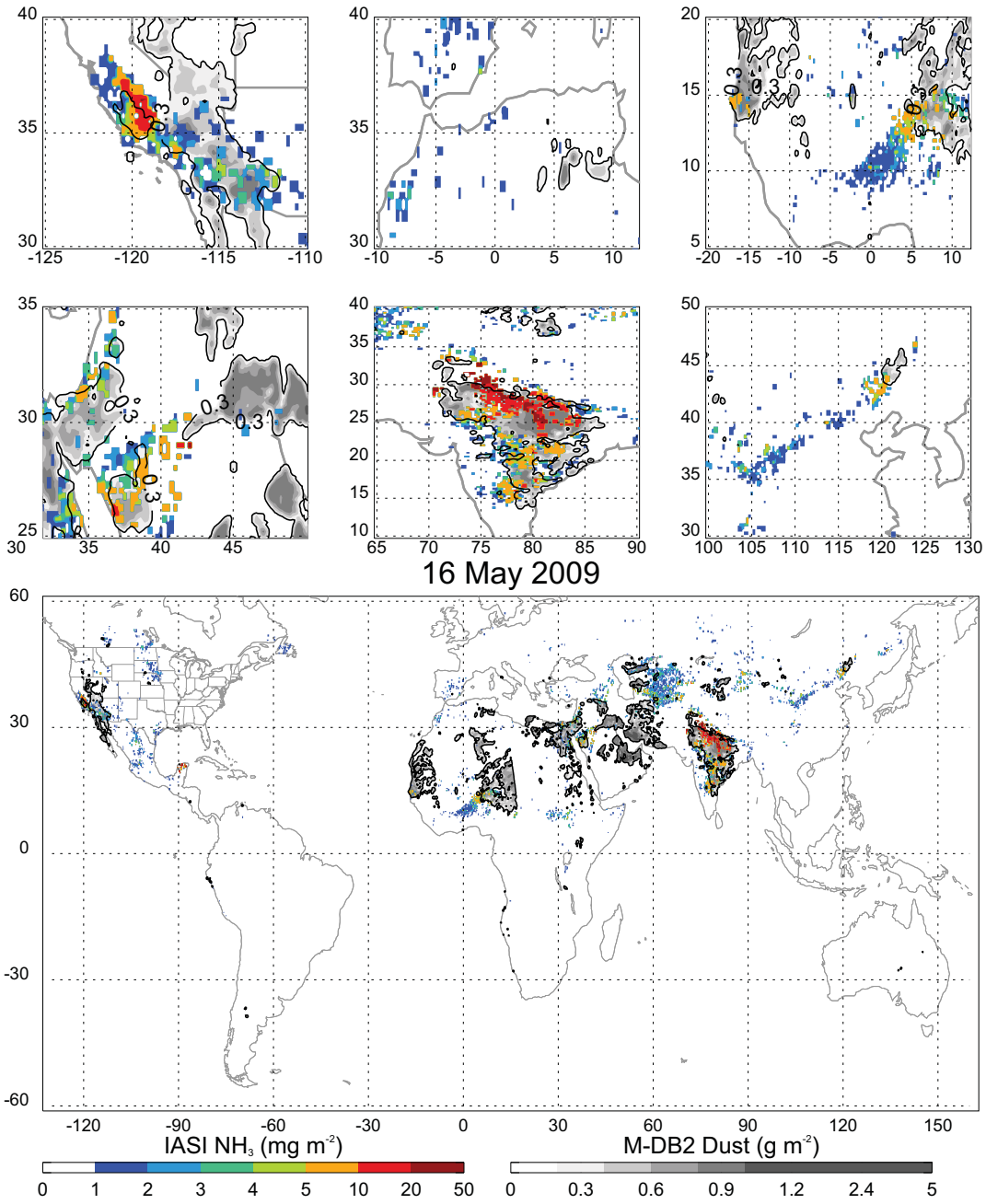

Fig. 1. Global (lower panel) distribution of M-DB2 dust column burden ($g\,m^{-2}$; grey shading) and IASI NH_3 column burden ($mg\,m^{-2}$; color shading), on 16 May 2009. The upper panels provide a zoom over 6 regions.

2.2 NH_3 column burden

Infrared radiances have been measured daily since the end of 2006 by the IASI instrument on board the EUMETSAT's polar orbiter MetOp. Clarisse et al. (2009) calculated the brightness temperature difference between radiances and converted it to column burden of NH_3. The first global distributions were obtained by averaging one year of measurements and 28 hotspot regions were identified. Here we use an improved product only available from April 2009 to March 2010. For this product NH_3 column burden is retrieved using a full Optimal Estimation scheme, as in Clarisse et al. (2010a), and similar to the processing algorithm used for other trace gases (Hurtmans et al., 2012). The retrieval is only carried out for the observations with a detectable spectral signal of NH_3. Hence, very low concentrations will not be measured. Similarly, when the contrast in temperatures between the ground and the atmosphere is weak, the IASI sensitivity to surface

concentrations is close to zero, and even significant NH_3 concentrations might be missed. While the IASI optimal estimation retrievals account for emissivity features by using temporal and spectrally resolved emissivity data (Zhou et al., 2011), some residual contamination due to emissivity features of windblown dust (Clarisse et al., 2010a) cannot be excluded. To minimize these, only those NH_3 retrievals with root mean square of the observed minus fitted spectrum below $2.8\,W\,cm^{-1}\,sr^{-1}$ were retained. This threshold value is close to the IASI instrumental noise in the relevant spectral range (Clerbaux et al., 2009).

Here we use the daily NH_3 column burden retrieved from April 2009 to March 2010 on each pixel (12 km diameter at nadir). Monthly averages are computed on a 0.25° by 0.25° grid. The value in each grid cell was obtained by averaging all observations within that cell. In grid cells where no measurements were made a value of zero was assigned. Although some biases cannot be avoided, this approach minimizes artifacts that would be introduced from interpolation of sparse data.

3 Global distribution of anthropogenic dust and NH_3

Figure 1 shows the column burden of M-DB2 dust, and IASI NH_3 on 16 May 2009. On that day significant amount of dust and NH_3 was observed to co-exist in different areas in the northern hemisphere. The main hot spots are in the southern part of the San Joaquin valley in California, the coastal region of Senegal, the Niger River Basin around Niamey (Niger), the Jordan River Basin, the Ganges River Basin, and the Horquin Sandy land in East China. All of these hotspots have been identified as anthropogenic dust sources by Ginoux et al. (2012). This snaphsot of dust and NH_3 examplifies their widespread co-existence over anthropogenic sources. The colocation of their sources suggests their mixing. However, the sources within the Niger River Basin are downwind of the Bodélé depression, one of the most active dust source on Earth (Prospero et al., 2002). MODIS swath on Aqua did not cover the depression on that day, which explains why Figure 1 does not show the Niger River Basin plume emanating from the Bodélé on that day. Similar occurrences of dust transport in elevated layers over Sahel, while NH_3 resides in the boundary layer, may falsely be interpreted as dust mixedintroduce with NH_3. On the other hand, it has been suggested from modeling studies with support from aircraft data that NH_3 may, in some cases, be transported in the free troposphere (Wang et al., 2008). Using vertical profile of aerosols from lidar in space satellite instruments may partially help, but their narrow field of view makes seldom their collocation with location specific small dust events.

We would like now to estimate the persistence of collocated sources an annual basis, and estimate the fraction of dust burden mixed with NH_3 for different types of land use.

Klein Goldewijk (2001) (KG) and Ramankutty and Foley (1999) (RF) have derived the global distribution of the fraction of pasture and cropland per 0.1 and 0.5 degree gridcell, respectively. KH derived land-use type from statistical information on national and sub-national level and population density, while RF used remote sensing ans statistical analysis. As in Ginoux et al. (2010), we use here KG land-use database, but will also compare our results using RF data.

We distinguish between natural and anthropogenic (agricultural) dust by assuming that the latter corresponds to dust over areas with more than 30 % land use. Natural dust is associated with less than 30 % land use. We further separate between cropland and pasture dust depending on which one has the largest fraction within a grid cell.

Figure 2 shows the annual mean column burden of M-DB2 dust, and IASI NH_3. We see that most of the "dust belt", defined by Prospero et al. (2002), is covered with at least $0.1\,g\,m^{-2}$ of dust. The Sahara desert is essentially characterized by natural dust while most of Sahel is associated with pasture except in Senegal, Burkina Faso, Niger and Nigeria where cropland dominates. In the Middle East, cropland is confined to some areas of Mesopotamia. In Central Asia, most anthropogenic dust is associated with pasture, while dust over cropland covers most of India and East China. In the Southern Hemisphere, dust over cropland is found in Argentina and Southeast Australia, and dust over pasture covers Patagonia and Central and Northeast Australia. Over the United States, dust over cropland is confined to the southern part of the San Joaquin Valley of California and the Midwest, and dust over pasture dominates the Southwest. Major differences of land-use fraction between KG and RF exist over the Saudi Arabian Peninsula and Australia, where land use is less than 30 % in case of RF database.

Inventory of global ammonia emissions indicates that 60 % comes from agriculture, with 1/3 from fertilizer and 2/3 from livestock sources (Beusen et al., 2008). Lifetime of gaseous NH_3 is about 22 h (Adams et al., 1999), which produces well defined hot spots centered over its sources. This is clearly apparent in Fig. 2 where NH_3 distribution is covering most cropland, which happens to be also source of dust (i.e. US Great Plains, Argentina, Sahel, Mediterranean coast, Mesopotamia, Uzbekistan, India, East China). The most pronounced feature is over the Indo-Gangetic basin, where dust and NH_3 column burden are greater than $0.5\,g\,m^{-2}$, and $0.5\,mg\,m^{-2}$, respectively.

The global annual mean dust burden from M-DB2 is 4.2 Tg, which is four times lower than the median value of 16 Tg derived by Huneeus et al. (2011) from 14 models, with values ranging from 6.8 to 29.5 Tg depending on the model. There are two major reasons for this discrepancy: one is due to uncertainty in ϵ in Eq. (1) and the other comes from M-DB2 retrieval over bright surface only. By excluding dark surfaces (i.e. oceans) transported dust is not included in our results. As we are interested to study dust over its sources, which are located over land, this is not an issue. Additionally,

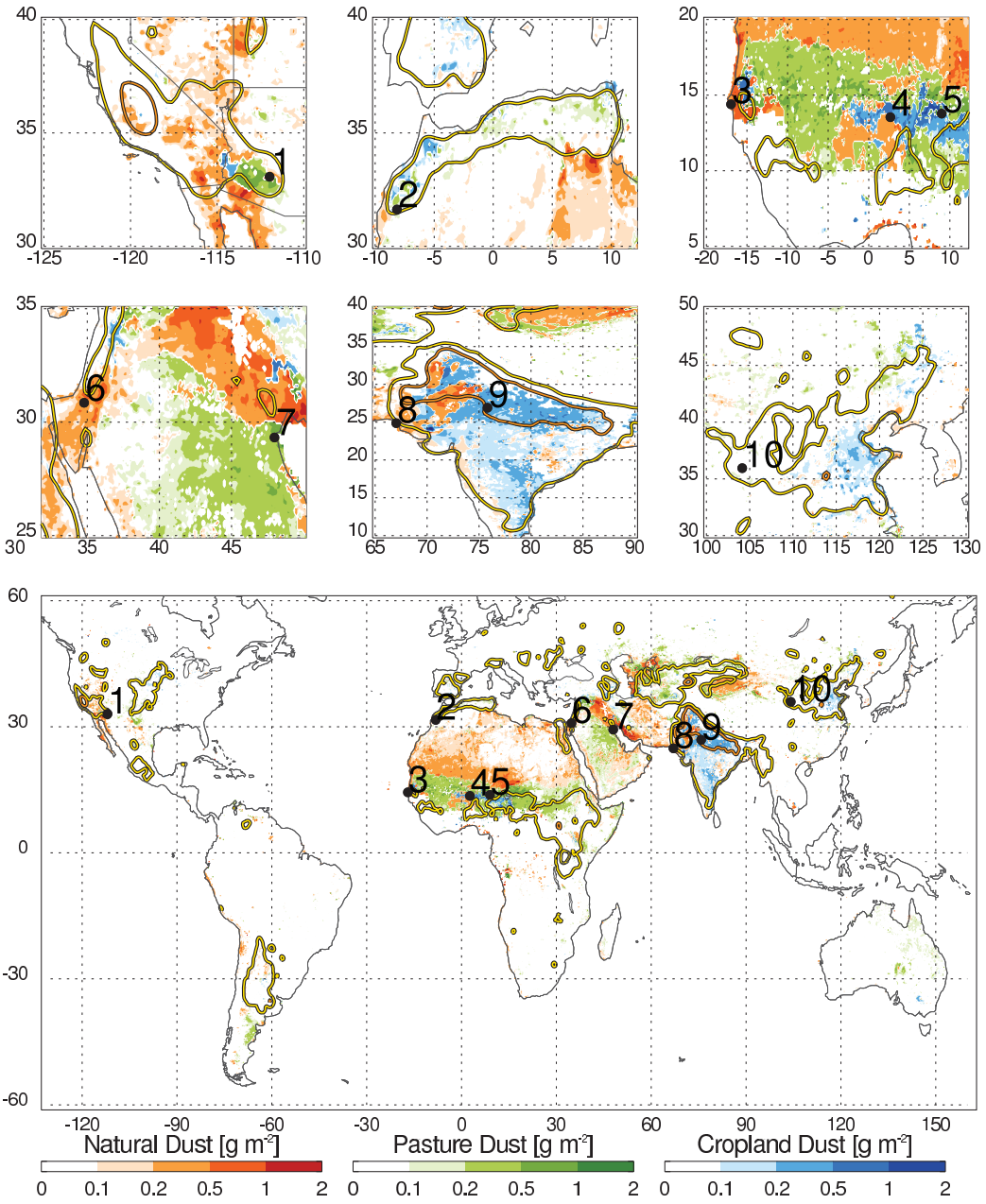

Fig. 2. Global (lower panel) annual mean distribution of M-DB2 dust column burden ($g\,m^{-2}$) over areas with less than 30 % (Natural Dust; red shading) and more than 30 % land-use -with an additional distinction between the prevalence of pasture over cropland (pasture dust; green shading) and cropland over pasture (cropland dust; blue shading), 0.5 (yellow contour) and 2.5 (orange contour) column burden ($mg\,m^{-2}$) of IASI NH_3, with the numbers 1 to 10 indicating the position of the AERONET sites of Fig. 4, and the upper panels providing a zoom over 6 regions.

we consider only one year while interannual variability of dust burden is of the order of 20 % (Ginoux et al., 2004).

4 Anthropogenic dust mixed with NH_3

In this section, we quantify the mixing of dust with NH_3 over agriculture at the global and continental scales.

The percentage of anthropogenic dust mixed with NH_3 over each landcover types is calculated by summing areas of each type where M-DB2 dust is mixed with detectable amount of IASI NH_3 (mass burden greater than $1\,mg\,m^{-2}$), and dividing by the total surface of that cover type where M-DB2 dust is present. We consider both KG and RF land-use databases. We see in Fig. 3 that, for both databases, the

Table 1. Annual mean total burden of M-DB2 dust (M_{DU}) in units of ktons as well as the fraction (%) of dust mixed with NH_3 over all land cover types (f^{tot}), cropland (f^{crop}), pasture (f^{past}), and with less than 30 % land-use (f^{nat}), for the Klein Goldewijk (2001) and Ramankutty and Foley (1999) (in italics) landuse datasets, over 9 regions which boundaries are defined by their minimum and maximum latitude (Lat) and longitude (Lon). Percentage fraction greater than 20 % are indicated in bold font.

Region	Lon Range	Lat Range	M_{DU}^{tot}	M_{DU}^{crop}	M_{DU}^{past}	M_{DU}^{nat}	f^{tot}	f^{crop}	f^{past}	f^{nat}
Global	130° W–160° E	60° S–60° N	4184	532–*579*	1622–*1422*	2029–*2183*	7–*7*	**22**–***21***	7–*8*	4–*4*
North America	125° W–70° W	20° N–50° N	128	9–*15*	85–*87*	33–*26*	11–*11*	19–*18*	11–*11*	10–*10*
South America	85° W–60° W	55° S–0° N	70	3–*5*	28–*26*	38–*39*	6–*6*	**26**–*18*	3–*11*	6–*10*
North Africa	20° W–35° E	5° N–40° N	1934	141–*165*	667–*627*	1126–*1142*	4–*4*	11–*10*	7–*6*	2–*2*
South Africa	5° E–50° E	35° S–5° N	95	2–*1*	70–*65*	24–*29*	5–*5*	13–*6*	5–*5*	4–*5*
West Asia	35° E–60° E	5° S–50° N	1000	72–*70*	431–*343*	498–*587*	4–*4*	8–*7*	5–*6*	4–*3*
Central Asia	60° E–100° E	5° N–30° N	334	223–*248*	0–*1*	111–*85*	**26**–***26***	**34**–***32***	0–***23***	12–*10*
East Asia	60° E–140° E	30° N–50° N	481	63–*59*	222–*206*	196–*216*	14–*14*	**25**–***26***	15–*16*	9–*8*
Australia	110° E–155° E	45° S–10° S	142	6–*3*	133–*78*	3–*61*	1–*1*	3–*3*	1–*1*	0–*0*

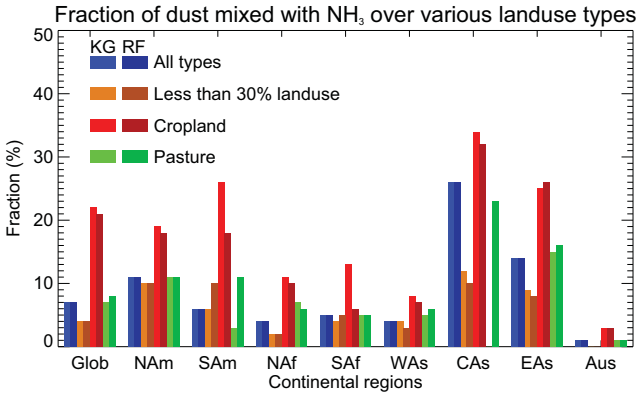

Fig. 3. Annual mean fraction (%) of M-DB2 dust column burden mixed with IASI NH_3 over all land surfaces (blue), areas with less than 30 % land-use (brown), cropland (red), and pasture (green) globally and over 8 continental regions, considering the Klein Goldewijk (2001) (KG) and Ramankutty and Foley (1999) (RF) land-use datasets, with the latter shown using darker colors.

largest percentage of mixed dust with NH_3 is over cropland globally, and for each sub-continents.

Table 1 provides more details on the annual burden and fraction of dust mixed with NH_3 over various continental regions and for KG and RF land-use databases. Globally, 7 % of dust is mixed with NH_3, which represents 310 ktons of dust. If we consider only croplands, we found 21–22 % of dust is mixed with NH_3, which corresponds to 115–122 ktons or 3 % of global dust burden (4.2 Tg), depending on the land-use database. The largest fraction of dust mixed with NH_3 (26 %) is observed over croplands of South and Central Asia subcontinent, with 32–34 % corresponding to 66–76 ktons, depending on the land-use database. The other area with significant amount of mixed dust is East Asia (67 ktons or 14 % of global burden) with 25–26 % from cropland. In North America, mixed dust represents only 14 ktons (11 % of North American dust burden) mostly from cropland (18–19 %). North Africa represents 46 % of global dust burden, but only 77 ktons (less than 2 % of global burden) is mixed with NH_3 with most of it over cropland.

5 Comparison with AERONET data

In order to evaluate M-DB2 derived column burden of dust, its value is compared with retrieval from inversion of Aerosol Robotic Network (AERONET) sunphotometer data. AERONET is a federated worldwide network of sunphotometers that are monitored and maintained at the NASA Goddard Space Flight Center (Holben et al., 1998). Dust particles are essentially greater than 1 μm radius (coarse mode), but about 10 % of dust mass, mostly clay, is submicron (fine mode) (Ginoux et al., 2001). The parameters of the size distribution for fine and coarse modes are retrieved by inversion of Almucantar measurements (Dubovik and King, 2000). Here we use the daily quality assured (Level 2) volume concentration for the coarse mode from 1 April 2009 to the end of March 2010 in order to coincide with IASI data.

The Angstrom wavelength exponent α is often used as an indicator of the dominance of one aerosol mode over the other. For example, using AERONET data, Eck et al. (1999) have shown that α values are generally lower than 0.5 in dusty environments and higher in polluted regions. To make sure that dust is the major aerosol contributing to the measured extinction, we extract coarse mode volume concentration when $\alpha < 0.5$. The volume concentration is then multiplied by the uncoated dry dust density (2600 $kg\,m^{-3}$) to convert it into column burden. Samples collected in different areas of North Africa contain between 2 and 6 % sulfate in volume (Wagner et al., 2012), which suggest an error of the order of 10 % in the density.

The AERONET retrieval algorithm in case of dust is described in details by Dubovik et al. (2006). Here, briefly, the algorithm assumes spherical particles, except when the Angstrom exponent is lower than 0.5, in which case spheroid models are used. For Angstrom less than 0.5, the estimated error is between 10 and 20 % for Level 2 data.

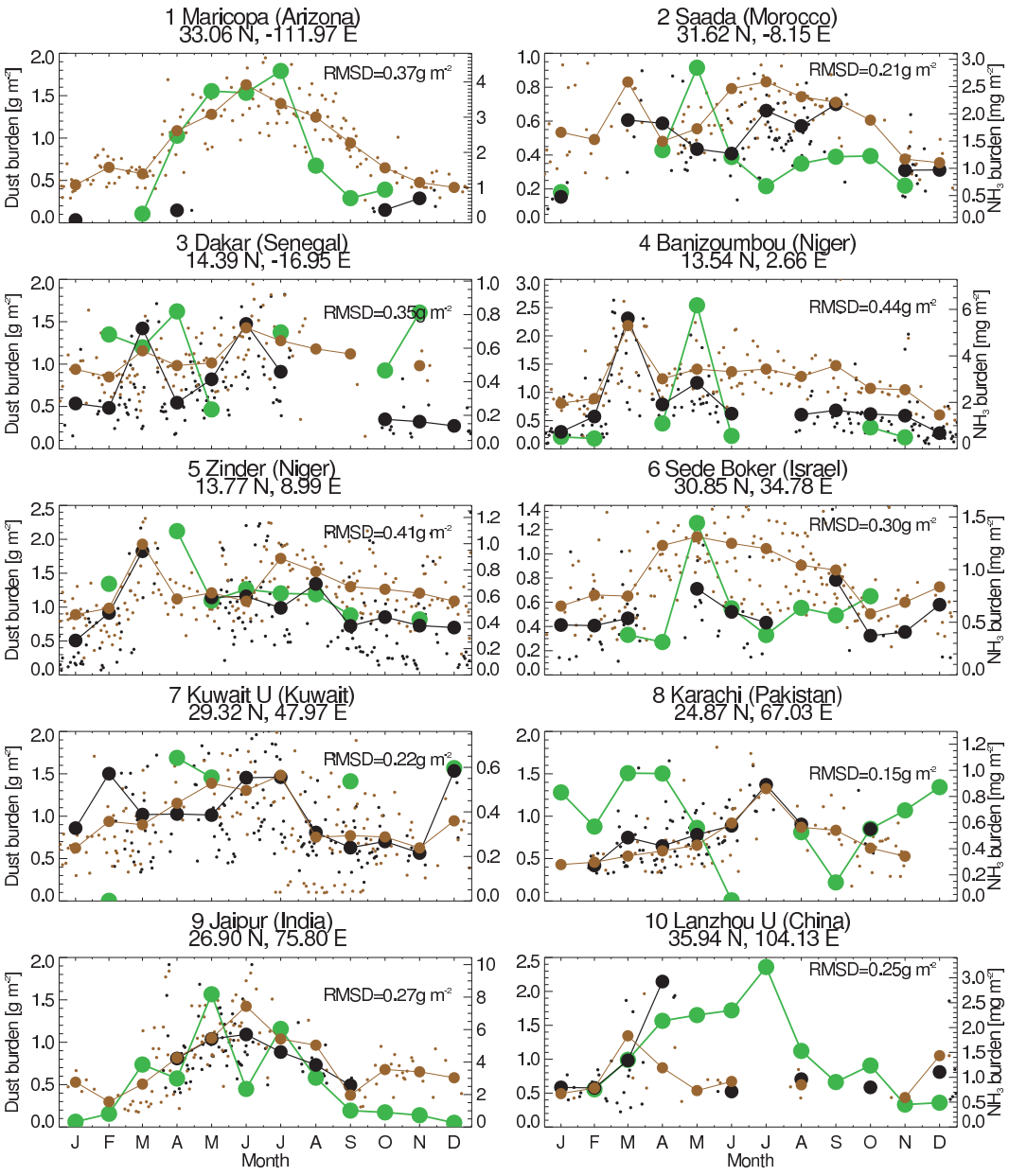

Fig. 4. Daily (small dots) and monthly (large dots) AERONET coarse mode column burden (black), M-DB2 dust burden (brown) in units of $g\,m^{-2}$ (left vertical axes), and IASI NH_3 column burden (green) in units of $mg\,m^{-2}$ (right vertical axes) at 10 AERONET sites. The root mean square difference (RMSD) in units of $g\,m^{-2}$ between monthly M-DB2 and AERONET mass column burden is provided in the upper right.

Ten AERONET sites have been selected based on the diversity of their geographical location over agriculture dominated areas. Satellite data within 25 km of the AERONET sites are used for this comparison.

Figure 4 shows the time series of daily and monthly dust column burden from M-DB2 and AERONET and monthly IASI NH_3 column burden at the selected sites from April 2009 to March 2010. The largest root mean square difference (RMSD) between AERONET and M-DB2 dust burden appears in Niger at Banizoumbou (RMSD = $0.44\,g\,m^{-2}$) and Zinder (RMSD = $0.41\,g\,m^{-2}$), but the mean values are also the largest at these sites. The highest monthly dust burden ($2.3\,g\,m^{-2}$) among all ten sites is observed in Banizoumbou (Niger) in March. African sites are characterized by two maxima of dust burden, one in March and the other in boreal summer (June-July-August). The seasonal variation of dust burden at the sites located in Sahel (south of 20° N) can be explained by the movement of the InterTropical Convergence

Zone (ITCZ) occupying its southernmost position (5° N) in December and its northernmost position (20° N) in July. As the ITCZ moves over these sites, dry air mass from the north is replaced by monsoon flow from the south bringing precipitation, which suppresses dust emission and removes dust particles from the atmosphere. Sharp changes of wind direction and relative humidity have been observed in mid-October and early May at Banizoumbou, as well as a maximum of dust optical depth in March and June (Rajot et al., 2008). Summer maximum of dust load at the Kuwait site has been associated with increased surface winds in summer (Sabbah, 2010). The RMSD ($0.22\,g\,m^{-2}$) is relatively low at that site, but is reaching $0.3\,g\,m^{-2}$ in Sede Boker (Israel). The summer maximum in Sede Boker has been associated with dust originating from the Arabian Peninsula and the Sahara (Israelevich et al., 2003). At the two sites in the Indo-Gangetic basin (Karachi and Jaipur), there is a pronounced maximum of dust load during the pre-monsoon season with monthly dust burden reaching up to $1.5\,g\,m^{-2}$. This seasonal variation corresponds to the climatological (2001–2009) cycle of coarse mode optical depth measured with sunphotometer over the Indo-Gangetic Plain (Giles et al., 2011). In China, dust activity peaks in spring (Prospero et al., 2002) but M-DB2 value underestimates AERONET data by a factor 2 in March. This large discrepancy may be due to the low number of observations during that month.

The summer maximum of IASI NH_3 observed in Maricopa has been attributed to the strong dependency of ammonia volatilization on surface temperature (Clarisse et al., 2010b). The similarity of NH_3 and dust cycle suggests also a dependency on wind speed on NH_3 volatilization.

In Africa, there is a distinct peak of IASI NH_3 in May which was also observed in surface concentration of NH_3 in Banizoumbou by Galy-Lacaux et al. (2001). They related the high concentration of ammonia in Banizoumbou to a local density gradient of animals grazing in pasture areas, but they did not discuss the origin of this pronounced peak in May. Except for this peak, the seasonal cycle of NH_3 in Africa is quite similar to the one of dust. The highest concentration of NH_3 is observed in India. The high level of NH_3 concentration in India compared to the rest of the world has already been shown by Dentener and Crutzen (1994) and later confirmed by Clarisse et al. (2009). The similarity of dust and NH_3 seasonal cycles at all these different sites, except for Karachi, suggests a common origin, such that NH_3 may be used as a tracer for anthropogenic dust. Next, we would like to detect potential differences in optical properties between natural and anthropogenic dust, in particular concerning the mass extinction efficiency.

6 Mass extinction efficiency of dust

6.1 Dependency on NH_3

Theoretical calculation using Mie theory indicates that the mass extinction efficiency ϵ of dust decreases when mixed with sulfate or nitrate (Bauer et al., 2007). As we have seen that NH_3 is a good tracer for anthropogenic dust, the influence of anthropogenic dust on ϵ should be correlated with NH_3 concentration.

To examine the existence of such effect on optical properties retrieved from sunphotometers, we extract all AERONET inversion Level 2 daily data from April 2009 to March 2010. As we are only interested in dusty cases, we restrict the data for days when α is lower than 0.5. To calculate the mass extinction efficiency we multiply the volume concentration retrieved from the inversion of AERONET data (Dubovik and King, 2000) by the mass density of uncoated dry dust ($2600\,kg\,m^{-3}$) and divide by the extinction measured directly by the sunphotometer. We have indicated in Sect. 3 a possible 10 % error in the density by considering uncoated dry dust. We selected the extinction at 670 nm because there are more instruments measuring at that wavelength than at 550 nm. The fine and coarse mode mass extinction efficiencies are calculated separately, using the corresponding retrieved volume concentration. These values are then clustered as a function of co-located (same day and within 25 km) IASI NH_3 concentration.

Figure 5 shows the daily values of mass extinction efficiency ϵ of fine (FMEE) and coarse (CMEE) modes at all AERONET sites with Angstrom exponent less than 0.5, as a function of NH_3 column burden and season. The mean values of FMEE and CMEE for different ranges of NH_3 concentrations are also provided in the Figure. We see a clear decrease of CMEE as NH_3 increases, with mean values at $0.62\,m^2\,g^{-1}$ for NH_3 less than $2\,mg\,m^{-2}$ and decreasing to $0.48\,m^2\,g^{-1}$ for NH_3 greater than $20\,mg\,m^{-2}$. On the other hand, there is a factor 3 variability of FMEE but apparently unrelated to NH_3 concentration. Considering NH_3 as a tracer of anthropogenic dust, these results suggest that the mass extinction efficiency of anthropogenic dust has a lower coarse mode mass extinction efficiency than natural dust, but has similar fine mode mass extinction as natural dust. So, the value of $\epsilon = 0.6\,m^2\,g^{-1}$ derived from Eq. (1) corresponds quite well to the mean value observed by AERONET sunphotometer in the case of natural dust.

Figure 5 shows that the variability of FMEE at Zinder Airport in summer is as large as a factor 3, still with the same range of NH_3 burden. Similarly, FMEE at Jaipur in spring varies by more than a factor 2 while NH_3 is ranging between 2 and $4\,mg\,m^{-2}$. There is clearly another factor controlling FMEE variability.

Sullivan et al. (2007) have shown that ammonium sulfate will preferentially accumulate on fine mode dust because H_2SO_4 reactions with dust depends on aerosol surface

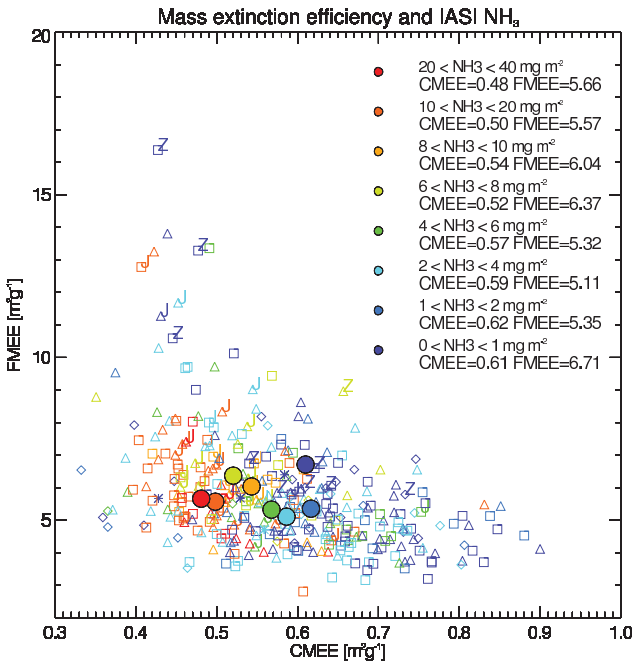

Fig. 5. Daily mass extinction efficiency ($m^2\,g^{-1}$) for coarse (CMEE) and fine (FMEE) modes at all AERONET stations from April 2009 to March 2010 when the Angstrom exponent is less than 0.5, and as a function of IASI NH_3 column burden for 8 ranges of values (colors), with mean values of FMEE and CMEE given in units of $m^2\,g^{-1}$ provided in upper right. The corresponding season is indicated by star (December-January-February), triangle (March-April-May), square (June-July-August), and diamond (September-October-November) symbols. The Zinder Airport and Jaipur AERONET sites are indicated by the letter Z and J, respectively.

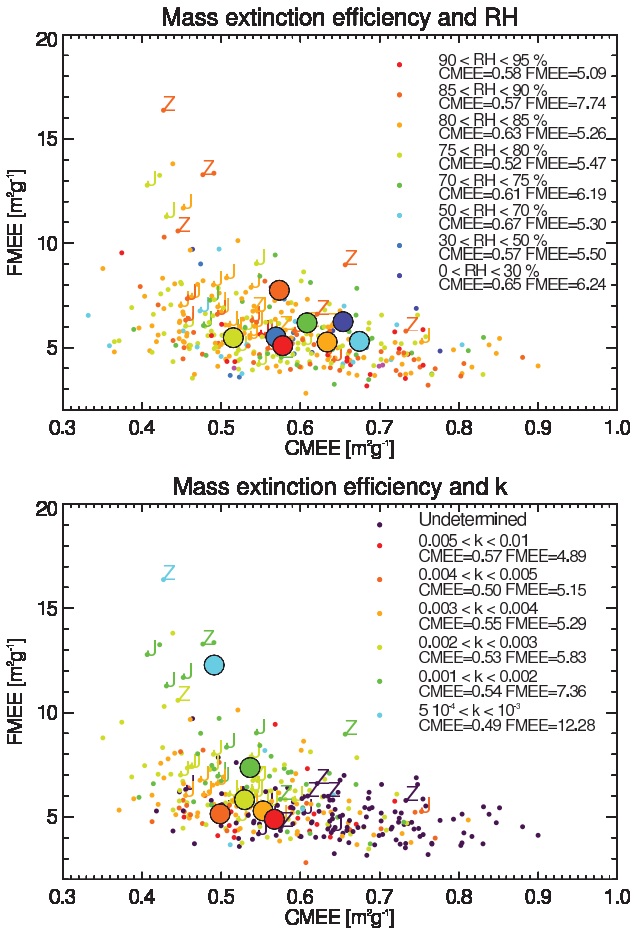

Fig. 6. Daily mass extinction efficiency ($m^2\,g^{-1}$) for coarse (CMEE) and fine (FMEE) modes at all AERONET stations from April 2009 to March 2010 when the Angstrom exponent is less than 0.5, and as a function of relative humidity at 925 mb (upper panel) and AERONET imaginary part of refractive index at 670 nm (lower panel). The range of RH and k values and the corresponding mean values of FMEE and CMEE, in units of $m^2\,g^{-1}$ are provided on the upper right of each panels. The Zinder Airport and Jaipur AERONET sites are indicated by the letter Z and J, respectively.

area to which fine mode contributes more than coarse mode. They further explained that these reactions will displace any preexisting nitrate back to the gas phase and will subsequently accumulate on the coarse mode. Ammonium salts were found to be internally mixed with dust, and are strongly correlated with the sum of acids in dust. Thus they demonstrated that ammonium predominantly accumulates in fine mode dust, and subsequently on coarse mode with increasing ammonium. As ammonium salts are hygroscopic particles, if they are mixed with dust then FMEE should be sensitive to relative humidity, which may explain the large variation of FMEE at one location and during the same season.

6.2 Dependency on RH

Hygroscopic growth of ammonium sulfate can increase ϵ by an order of magnitude from its deliquescence point to high ($> 90\,\%$) relative humidity (Tang, 1996). We should also expect some growth of fine dust internally mixed with sulfate, although not as pronounced as pure sulfate because dust itself is hydrophobic.

Opposite to natural dust sources, located in arid or semi-arid regions, most anthropogenic sources are influenced by moist air from monsoon flow (Ginoux et al., 2012), which may generate hygroscopic growth of aerosols. But if these sources are instead influenced by dry winds or dust is in elevated layers, no growth should be expected.

To verify that fine mode dust is mixed with NH_3 and grows hygroscopically, we extract the daily boundary layer (925 hPa) relative humidity (RH) from NCEP/NCAR reanalysis (Kalnay et al., 1996) at the AERONET sites for the corresponding days and locations. Figure 6 (upper panel) is similar to Fig. 5 but each data is color coded as a function of RH. The Figure shows no apparent dependency of mean FMEE on RH although RH varies below and above the deliquescence point of $(NH_4)_2SO_4$ (Haywood and Ramawsamy,

1998). At Zinder airport, the relative humidity in summer does not vary considerably ranging from 85 and 90 %. Similarly, at the Jaipur site in spring, RH is below the deliquescence point as RH values varies between 75 and 80 %. These results indicate a weak dependency of FMEE on hygroscopic growth in these measurements, but it does not mean that there is none.

Several reasons may hinder mesurable changes of FMEE by RH. These include the dependency of the deliquescence of ammonium salts on hysteresis (Martin et al., 2000, 2008), and the presence of other compounds, such as organics (Wang et al., 2008), or that dust and NH_3 are in different vertical layers. We have also to consider that monsoon conditions are often accompanied by clouds, which are discarded from AERONET Level 2 data by the cloud screening algorithm. In addition, fine mode mass extinction efficiency is mostly sensitive to change in scattering and absorption properties rather than size. The opposite is true for the coarse mode mass extinction efficiency (Seinfeld and Pandis, 1998). So, it may be more effective to study variability of FMEE based on absorption property.

6.3 Dependency on *k*

Mass extinction efficiency of aerosol depends on the refractive index, whose imaginary part is related to its absorption property. Figure 6 (lower panel) shows the dependency of FMEE and CMEE on the imaginary part of the refractive index (k) at 670 nm. As absorption increases FMEE decreases from about 12 to 5 $m^2\,g^{-1}$. The decrease of FMEE with increasing k appears clearly at the two AERONET sites (Zinder airport and Jaipur).

Analysis of dust samples collected at different locations in North Africa indicates k values at 655 nm ranging from $0.0016\,i$ to $0.0065\,i$ (Wagner et al., 2012), which is covering most of our results. The size resolved composition of the soil samples by Wagner et al. (2012) indicates a much larger abundance of sulfate and other non-crustal elements in the fine mode, with sulfate volume abundance varying from 2 to 6 %. The authors related the variability of k to mineralogical composition. In fact, mineralogy determines not only the amount of iron, and thus absorption by dust, but also the chemical processing by ammonium salts. Sullivan et al. (2007) have shown that sulfate is more strongly associated with aluminosilicate-rich dust particles while nitrate and chloride are more associated with calcite-rich dust. Iron is essentially associated with aluminosilicates. This double influence of mineralogy may explain the variability of FMEE. The strong dependency of k to source location has been shown for Saharan dust using backtrajectory analysis (McConnell et al., 2010). Here, we show that such variation is also linked to the anthropogenic origin of dust due to its mixing with ammonium salts or other acidic components from organic soils used for agriculture.

We can conclude from Figs. 5 and 6, that over source areas, natural dust mass extinction efficiency is 0.6 $m^2\,g^{-1}$ for coarse mode, and decreases to 0.4–0.5 $m^2\,g^{-1}$ for anthropogenic dust, mostly due to mixing with ammonium salts or organics from fertilizer. On the other hand, for fine mode dust mineralogy is a major factor controlling the mass extinction efficiency.

7 Conclusions

The global distributions of dust and NH_3 column burden have been compared to determine: (1) if they are mixed over dust sources, (2) the global and regional fractions of dust mixed with NH_3, and (3) the effect of such mixing on dust optical properties.

To achieve these objectives, dust optical depth (DOD) derived from M-DB2 aerosol products has been converted into column burden by dividing DOD by a theoretical mass extinction efficiency. The distribution of M-DB2 dust column burden is then compared to NH_3 retrieved from the IASI satellite data.

Using two different land-use datasets we found substantial similarity between the annual mean distribution of dust and NH_3 burdens, particularly over croplands. The mass of dust mixed with NH_3 represents 7 to 8 % of the global mass estimated to be 4.1 Tg over dust sources, depending on the land-use dataset. Over croplands mixed dust represents 22 % globally, with only 1 % difference between land-use datasets. On a seasonal basis, the maximum mixing is observed in spring with almost 30 % of dust over cropland mixed with NH_3. Among the different continents, the Indian subcontinent has the largest fraction of dust mixed with NH_3 (26 %). Our results indicate that NH_3 is a good tracer for anthropogenic dust.

Comparison of dust column burden retrieved from M-DB2 and sunphotometers at 10 AERONET sites, spread over different continents, indicates good agreement in Africa and Asia but large overestimation of M-DB2 values over Arizona and to a lesser extend in Israel.

To study the difference between anthropogenic and natural dust on optical properties, we derived the mass extinction efficiency for the coarse and fine mode at all AERONET sites. Only dusty days with Angstrom exponent less than 0.5 were considered. By collocating IASI NH_3 column burden with AERONET data, we found that ϵ is 0.6 $m^2\,g^{-1}$ for the coarse mode, and it decreases to a minimum of 0.4–0.5 $m^2\,g^{-1}$ when mixed with concentration of NH_3 in excess of 20 $mg\,m^{-2}$. This represents a 20 % decrease with a ten-fold increase of NH_3 concentration. The mass extinction efficiency for fine mode is ten times higher than for coarse mode of unmixed dust, with no clear dependency on NH_3 concentration or relative humidity. Instead, we found a sensitivity to the imaginary part of the refractive index that we attributed to mineralogy and mixing with other aerosols. In view of previous

analysis of in-situ data, we related this decrease of coarse mode ϵ as a result of the accumulation of purely scattering ammonium, while for the fine mode the amount of absorption is determined by the mineralogical composition. Mineralogical composition determines not only the amount of absorptive iron but also the accumulation of ammonium salts.

The relatively weak change of mass extinction efficiency is in agreement with a previous model study (Bauer et al., 2007). However, such study considered dust aging during transport whereas we have considered here dust co-located mostly over croplands with IASI NH_3 hot spots. The existence of mixed dust with NH_3 over large areas implies that a significant amount of dust is already mixed with ammonium salt before its long range transport and cloud processing. This in turn will affect dust lifetime, and its interactions with radiation, cloud properties, and ocean biogeochemistry.

Acknowledgements. We would like to thank Massimo Bollasina, Songmiao Fan and two anonymous reviewers for providing fruitful comments on the manuscript. We thank the AERONET program for establishing and maintaining the sunphotometer sites used in this study, in particular Brent Holben for the Maricopa and Karachi sites, Bernadette Nougenot and Benoit Duchemin for the Saada site, Didier Tanré for the Banizoumbou and Dakar sites, Bernadette Chatenet and Jean-Louis Rajot for the Zinder Airport site, Arnion Karielli for the Sede Boker site, Hala Al-Jassar for the Kuwait University site, Naif Al-Abbadi for the Solar Village site, Brent Holben for the Karachi site, Swagata Payra for the Jaipur site, and Jianping Huang for the SACOL (University of Lanzhou) site. IASI has been developed and built under the responsibility of the Centre National d'Etudes Spatiales (CNES, France). It is flown on board the MetOp satellites as part of the EUMETSAT Polar System. The IASI L1 data are received through the EUMETCast near-real-time data distribution service. L. Clarisse, P. F. Coheur and M. Van Damme are respectively Postdoctoral Researcher (Chargé de Recherches), Research Associate (Chercheur Qualifié) and F.R.I.A. grant holder with F.R.S.-FNRS. The LATMOS team is grateful to CNES for scientific collaboration and financial support. The research in Belgium was funded by the Belgian State Federal Office for Scientific, Technical and Cultural Affairs, and the European Space Agency (ESA-Prodex arrangements). Financial support by the Actions de Recherche Concertées (Communauté Française de Belgique) is also acknowledged. D. Hurtmans is acknowledged for developing the IASI retrieval processing chain.

Edited by: D. Tanré

References

Adams, P. J., Seinfeld, J. H., and Koch, D. M.: Global concentrations of tropospheric sulfate, nitrate, and ammonium aerosol simulated in a general circulation model, J. Geophys. Res., 104, 13791–13823, doi:10.1029/1999JD900083, 1999.

Bauer, S. E., Mishchenko, M. I., Lacis, A. A., Zhang, S., Perlwitz, J., and Metzger, S. M.: Do sulfate and nitrate coatings on mineral dust have important effects on radiative properties and climate modeling?, J. Geophys. Res., 112, D06307, doi:10.1029/2005JD006977, 2007.

Beusen, A. H. W., Bouwman, A. F., Heuberger, P. S. C., Van Drecht, G., and Van Der Hoek, K. W.: Bottom-up uncertainty estimates of global ammonia emissions from global agricultural production systems, Atmos. Environ., 42, 6067–6077, doi:10.1016/j.atmosenv.2008.03.044, 2008.

Chen, G., Ziemba, L. D., Chu, D. A., Thornhill, K. L., Schuster, G. L., Winstead, E. L., Diskin, G. S., Ferrare, R. A., Burton, S. P., Ismail, S., Kooi, S. A., Omar, A. H., Slusher, D. L., Kleb, M. M., Reid, J. S., Twohy, C. H., Zhang, H., and Anderson, B. E.: Observations of Saharan dust microphysical and optical properties from the Eastern Atlantic during NAMMA airborne field campaign, Atmos. Chem. Phys., 11, 723–740, doi:10.5194/acp-11-723-2011, 2011.

Clarisse, L., Clerbaux, C., Dentener, F., Hurtmans, D., and Coheur, P. F.: Global ammonia distribution derived from infrared satellite observations, Nat. Geosci., 2, 479–483, doi:10.1038/ngeo551, 2009.

Clarisse, L., Hurtmans, D., Prata, A. J., Karagulian, F., Clerbaux, C., De Mazière, M., and Coheur, P.-F.: Retrieving radius, concentration, optical depth, and mass of different types of aerosols from high-resolution infrared nadir spectra, Appl. Optics, 49, 3713–3722, 2010a.

Clarisse, L., Shephard, M. W., Dentener, F., Hurtmans, D., Cady-Pereira, K., Karagulian, F., Van Damme, M., Clerbaux, C., and Coheur, P.-F.: Satellite monitoring of ammonia: a case study of the San Joaquin Valley, J. Geophys. Res., 115, D13302, doi:10.1029/2009JD013291, 2010b.

Clerbaux, C., Boynard, A., Clarisse, L., George, M., Hadji-Lazaro, J., Herbin, H., Hurtmans, D., Pommier, M., Razavi, A., Turquety, S., Wespes, C., and Coheur, P.-F.: Monitoring of atmospheric composition using the thermal infrared IASI/MetOp sounder, Atmos. Chem. Phys., 9, 6041–6054, doi:10.5194/acp-9-6041-2009, 2009.

Dentener, F. J. and Crutzen, P. J.: A three-dimensional model of the global ammonia cycle, J. Atmos. Chem., 19, 331–369, 1994.

Dubovik, O. and King, M. D.: A flexible inversion algorithm for retrieval of aerosol optical properties from Sun and sky radiance measurements, J. Geophys. Res., 105, 20673–20696, 2000.

Dubovik, O., Sinyuk, A., Lapyonok, T., Holben, B. N., Mishchenko, M., Yang, P., Eck, T. F., Volten, H., Munõz, O., Veihelmann, B., van der Zande, W. J., Leon, J.-F., Sorokin, M., and Slutsker, I.: Application of spheroid models to account for aerosol particle nonsphericity in remote sensing of desert dust, J. Geophys. Res., 111, D11208, doi:10.1029/2005JD006619, 2006.

Eck, T. F., Holben, B. N., Reid, J. S., Dubovik, O., Smirnov, A., O'Neill, N. T., Slutsker, I., and Kinne, S.: Wavelength dependence of the optical depth of biomass burning, urban, and desert dust aerosols, J. Geophys. Res., 104, 31333–31349, 1999.

Fairlie, T. D., Jacob, D. J., Dibb, J. E., Alexander, B., Avery, M. A., van Donkelaar, A., and Zhang, L.: Impact of mineral dust on nitrate, sulfate, and ozone in transpacific Asian pollution plumes, Atmos. Chem. Phys., 10, 3999–4012, doi:10.5194/acp-10-3999-2010, 2010.

Forster, P., Ramaswamy, V., Artaxo, P., Berntsen, T., Betts, R., Fahey, D. W., Haywood, J., Lean, J., Lowe, D. C., Myhre, G., Nganga, J., Prinn, R., Raga, G., Schulz, M., Van Dorland, R., Bodeker, G., Boucher, O., Collins, W. D., Conway, T. J., Dlugo-

kencky, E., Elkins, J. W., Etheridge, D., Foukal, P., Fraser, P., Geller, M., Joos, F., Keeling, C. D., Kinne, S., Lassey, K., Lohmann, U., Manning, A. C., Montzka, S., Oram, D., O'Shaughnessy, K., Piper, S., Plattner, G.-K., Ponater, M., Ramankutty, N., Reid, G., Rind, D., Rosenlof, K., Sausen, R., Schwarzkopf, D., Solanki, S. K., Stenchikov, G., Stuber, N., Takemura, T., Textor, C., Wang, R., Weiss, R., Whorf, T.: Changes in atmospheric constituents and in radiative forcing, in: Climate Change 2007: the Physical Science Basis, Contribution of Working Group I to the Fourth Assessment Report of the Intergovernmental Panel on Climate Change, edited by: Solomon, S., Qin, D., Manning, M., Chen, Z., Marquis, M., Averyt, K. B., Tignor, M., et al., Cambridge University Press, Cambridge, 129–234, 2007.

Galy-Lacaux, C., Carmichael, G. R., Song, C. H., Lacaux, J. P., Al Ourabi, H., and Modi, A. I.: Heterogeneous processes involving nitrogenous compounds and Saharan dust inferred from measurements and model calculations, J. Geophys. Res., 106, 12559–12578, doi:10.1029/2000JD900778, 2001.

Giles, D. M., Holben, B. N., Tripathi, S. N., Eck, T. F., Newcomb, W. W., Slutsker, I., Dickerson, R.R., Thompson, A. M., Mattoo, S., Wang, S.-H., Singh, R. P., Sinyuk, A., Schafer, J. S.: Aerosol properties over the Indo-Gangetic Plain: a mesoscale perspective from the TIGERZ experiment, J. Geophys. Res., 116, D18203, doi:10.1029/2011JD015809, 2011.

Ginoux, P., Chin, M., Tegen, I., Prospero, J. M., Holben, B., Dubovik, O., and Lin, S.-J.: Sources and distributions of dust aerosols simulated with the GOCART model, J. Geophys. Res., 106, 20255–20274, 2001.

Ginoux, P., Prospero, J. M., Torres, O., and Chin, M.: Long-term simulation of global dust distribution with the GOCART model: correlation with the North Atlantic Oscillation, Environ. Model. Soft., 19, 113–128, doi:10.1016/S1364-8152(03)00114-2, 2004.

Ginoux, P., Garbuzov, D., and Hsu, H. C.: Identification of anthropogenic and natural dust sources using Moderate Resolution Imaging Spectroradiometer (MODIS) Deep Blue level 2 data, J. Geophys. Res., 115, D05204, doi:10.1029/2009JD012398, 2010.

Ginoux, P., Prospero, J. M., Gill, T. E., Hsu, N. C., and Zhao, M.: Global scale attribution of anthropogenic and natural dust sources and their emission rates based on MODISD Deep Blue aerosol products, Rev. Geophys., doi:10.1029/2012RG000388, 2012.

Hansell Jr., R. A., Reid, J. S., Tsay, S. C., Roush, T. L., and Kalashnikova, O. V.: A sensitivity study on the effects of particle chemistry, asphericity and size on the mass extinction efficiency of mineral dust in the earth's atmosphere: from the near to thermal IR, Atmos. Chem. Phys., 11, 1527–1547, doi:10.5194/acp-11-1527-2011, 2011.

Haywood, J. M. and Ramaswamy, V.: Global sensitivity studies of the direct radiative forcing due to anthropogenic sulfate and black carbon aerosols, J. Geophys. Res., 103, 6043–6058, doi:10.1029/97JD03426, 1998.

Holben, B. N., Eck, T. F., Slutsker, I., Tanré, D., Buis, J. P., Setzer, A., Vermote, E., Reagan, J. A., Kaufman, Y. J., Nakajima, T., Lavenu, F., Jankowiak, I., and Smirnov, A.: AERONET – a federated instrument network and data archive for aerosol characterization, Remote Sens. Environ., 66, 1–16, 1998.

Hsu, N. C., Tsay, S. C., King, M., and Herman, J. R.: Aerosol properties over bright-reflecting source regions, IEEE T. Geosci. Remote, 42, 557–569, 2004.

Hsu, N. C., Tsay, S.-C., King, M., and Herman, J. R.: Deep Blue retrievals of Asian aerosol properties during ACE-Asia, IEEE T. Geosci. Remote, 44, 3180–3195, 2006.

Huneeus, N., Schulz, M., Balkanski, Y., Griesfeller, J., Prospero, J., Kinne, S., Bauer, S., Boucher, O., Chin, M., Dentener, F., Diehl, T., Easter, R., Fillmore, D., Ghan, S., Ginoux, P., Grini, A., Horowitz, L., Koch, D., Krol, M. C., Landing, W., Liu, X., Mahowald, N., Miller, R., Morcrette, J.-J., Myhre, G., Penner, J., Perlwitz, J., Stier, P., Takemura, T., and Zender, C. S.: Global dust model intercomparison in AeroCom phase I, Atmos. Chem. Phys., 11, 7781–7816, doi:10.5194/acp-11-7781-2011, 2011.

Hurtmans, D., Coheur, P.-F., Wespes, C., Clarisse, L., Scharf, O., Clerbaux, C., Hadji-Lazaro, J., George, M., and Turquety, S.: FORLI radiative transfer and retrieval code for IASI, J. Quant. Spectrosc. Ra., 113, 1391–1408, doi:10.1016/j.jqsrt.2012.02.036, 2012.

Israelevich, P. L., Levin, Z., Joseph, J. H., and Ganor, E.: Desert aerosol transport in the Mediterranean region as inferred from the TOMS aerosol index, J. Geophys. Res., 107, 4572, doi:10.1029/2001JD002011, 2003.

Jordan, C. E., Dibb, J. E., Anderson, B. E., and Fuelberg, H. E.: Uptake of nitrate and sulfate on dust aerosols during TRACE-P, J. Geophys. Res., 108, 8817, doi:10.1029/2002JD003101, 2003.

Kalnay, E., Kanamitsu, M., Kistler, R., Collins, W., Deaven, D., Gandin, L., Iredell, M., Saha, S., White, G., Woollen, J., Zhu, Y., Chelliah, M., Ebisuzaki, W., Higgins, W., Janowiak, J., Mo, K. C., Ropelewski, C., Wang, J., Leetmaa, A., Reynolds, R., Jenne, R., Joseph, D.: The NCEP/NCAR 40-year Reanalysis Project, B. Am. Meteorol. Soc., 77, 437–471, 1996.

Kaufman, Y. J., Koren, I., Remer, L. A., Tanré, D., Ginoux, P., and Fan, S.: Dust transport and deposition observed from the Terra-Moderate Resolution Imaging Spectroradiometer (MODIS) spacecraft over the Atlantic Ocean, J. Geophys. Res., 110, D10S12, doi:10.1029/2003JD004436, 2005.

Klein Goldewijk, K.: Estimating global land use change over the past 300 years: the HYDE database, Global Biogeochem. Cy., 15, 417–433, 2001.

Lesins, G., Chylek, P., and Lohmann, U.: A study of internal and external mixing scenarios and its effect on aerosol optical properties and direct radiative forcing, J. Geophys. Res., 107, 4094, doi:10.1029/2001JD000973, 2002.

Levin, Z., Ganor, E., and Gladstein, V.: The effects of desert particles coated with sulfate on rain formation in the Eastern Mediterranean, J. Appl. Meteorol., 35, 1511–1523, 1996.

Li, X., Maring, H. B., Savoie, D., Voss, K., and Prospero, J. M.: Dominance of mineral dust in aerosol light-scattering in the North Atlantic trade winds, Nature, 380, 416–419, 1996.

Martin, S. T.: Phase transitions of aqueous atmospheric particles, Chem. Rev., 100, 3403–3453, doi:10.1021/cr990034t, 2000.

Martin, S. T., Rosenoern, T., Chen, Q., and Collins, D. R.: Phase changes of ambient particles in the Southern Great Plains of Oklahoma, Geophys. Res. Lett., 35, L22801, doi:10.1029/2008GL035650, 2008.

McConnell, C. L., Formenti, P., Highwood, E. J., and Harrison, M. A. J.: Using aircraft measurements to determine the refractive index of Saharan dust during the DODO Experiments, Atmos. Chem. Phys., 10, 3081–3098, doi:10.5194/acp-10-3081-2010, 2010.

Meskhidze, N., Chameides, W. L., Nenes, A., and Chen, G.: Iron mobilization in mineral dust: can anthropogenic SO_2 emissions affect ocean productivity?, Geophys. Res. Lett., 30, 2085, doi:10.1029/2003GL018035, 2003.

Prospero, J. M., Ginoux, P., Torres, O., Nicholson, S. E., and Gill, T. E.: Environmental characterization of global sources of atmospheric soil dust identified with the Nimbus 7 Total Ozone Mapping Spectrometer (TOMS) absorbing aerosol product, Rev. Geophys., 40, 1002, doi:10.1029/2000RG000095, 2002.

Rajot, J. L., Formenti, P., Alfaro, S., Desboeufs, K., Chevaillier, S., Chatenet, B., Gaudichet, A., Journet, E., Marticorena, B., Triquet, S., Maman, A., Mouget, N., Zakou, A.: AMMA dust experiment: an overview of measurements performed during the dry season special observation period (SOP0) at the Banizoumbou (Niger) supersite, J. Geophys. Res., 113, D00C14, doi:10.1029/2008JD009906, 2008.

Ramankutty, N., and Foley, J.: Estimating Historical Changes in Global Land Cover: Croplands from 1700 to 1992, Global Biogeochem. Cycles, 13, 997–1028, doi:10.1029/1999GB900046, 1999.

Sabbah, I.: Impact of aerosol on air temprature in Kuwait, Atmos. Environ., 97, 303–314, 2010.

Salam, A., Lesins, G., and Lohmann, U.: Laboratory study of heterogeneous ice nucleation in 10 deposition mode of montmorillonite mineral dust particles aged with ammonia, sulfur dioxide, and ozone at polluted atmospheric concentrations, Air Qual. Atmos. Health, 1, 135–142, doi:10.1007/s11869-008-0019-6, 2008.

Seinfeld, J. H. and Pandis S. N.: Atmospheric Chemistry and Physics: from Air Pollution to Climate Change, John Wiley, New York, USA, 1326 pp., 1998.

Shi, Z., Zhang, D., Hayashi, M., Ogata, H., Ji, H., and Fujiie, W.: Influences of sulfate and nitrate on the hygroscopic behaviour of coarse dust particles, Atmos. Environ., 42, 822–827, doi:10.1016/j.atmosenv.2007.10.037, 2008.

Sullivan, R. C., Guazzotti, S. A., Sodeman, D. A., and Prather, K. A.: Direct observations of the atmospheric processing of Asian mineral dust, Atmos. Chem. Phys., 7, 1213–1236, doi:10.5194/acp-7-1213-2007, 2007.

Sullivan, R. C., Petters, M. D., DeMott, P. J., Kreidenweis, S. M., Wex, H., Niedermeier, D., Hartmann, S., Clauss, T., Stratmann, F., Reitz, P., Schneider, J., and Sierau, B.: Irreversible loss of ice nucleation active sites in mineral dust particles caused by sulphuric acid condensation, Atmos. Chem. Phys., 10, 11471–11487, doi:10.5194/acp-10-11471-2010, 2010.

Tang, I. N.: Chemical and size effects of hygroscopic aerosols on light scattering coefficients, J. Geophys. Res., 101, 19245–19250, 1996.

Tanré, D., Kaufman, Y. J., Holben, B. N., Chatenet, B., Karnieli, A., Lavenu, F., Blarel, L., Dubovik, O., Remer, L. A., and Smirnov, A.: Climatology of dust aerosol size distribution and optical properties derived from remotely sensed data in the solar spectrum, J. Geophys. Res., 106, 18205–18217, doi:10.1029/2000JD900663, 2001.

Usher, C. R., Michel, A. E., and Grassian, V. H.: Reactions on mineral dust, Chem. Rev., 103, 4883–4939, doi:10.1021/cr020657y, 2003.

Wagner, R., Ajtai, T., Kandler, K., Lieke, K., Linke, C., Müller, T., Schnaiter, M., and Vragel, M.: Complex refractive indices of Saharan dust samples at visible and near UV wavelengths: a laboratory study, Atmos. Chem. Phys., 12, 2491–2512, doi:10.5194/acp-12-2491-2012, 2012.

Wang, J., Hoffmann, A. A., Park, R. J., Jacob, D. J., and Martin, S. T.: Global distribution of solid and aqueous sulfate aerosols: Effect of the hysteresis of particle phase transitions, J. Geophys. Res., 113, D11206, doi:10.1029/2007JD009367, 2008.

Zhou, D. K., Larar, A. M., Liu, X., Smith, W. L., Strow, L. L., Yang, P., Schlüssel, P., and Calbet, X.: Global land surface emissivity retrieved from satellite ultraspectral IR measurements, IEEE T. Geosci. Remote, 49, 1277–1290, 2011.